Soft Matter

PAPER

View Article Online
View Journal | View Issue

Cite this: *Soft Matter*, 2016, 12, 5041

Translocation dynamics of knotted polymers under a constant or periodic external field†

Vivek Narsimhan,[a] C. Benjamin Renner[b] and Patrick S. Doyle*[a]

Received 2nd March 2016,
Accepted 6th May 2016

DOI: 10.1039/c6sm00545d

www.rsc.org/softmatter

We perform Brownian dynamics simulations to examine how knots alter the dynamics of polymers moving through nanopores under an external field. In the first part of this paper, we study the situation when the field is constant. Here, knots halt translocation above a critical force with jamming occurring at smaller forces for twist topologies compared to non-twist topologies. Slightly below the jamming transition, the polymer's transit times exhibit large fluctuations. This phenomenon is an example of the knot's molecular individualism since the conformation of the knot plays a large role in the chain's subsequent dynamics. In the second part of the paper, we study the motion of the chain when one cycles the field on and off. If the off time is comparable to the knot's relaxation time, one can adjust the swelling of the knot at the pore and hence design strategies to ratchet the polymer in a controllable fashion. We examine how the off time affects the ratcheting dynamics. We also examine how this strategy alters the fluctuations in the polymer's transit time. We find that cycling the force field can reduce fluctuations near the knot's jamming transition, but can enhance the fluctuations at very high forces since knots get trapped in metastable states during the relaxation process. The latter effect appears to be more prominent for non-torus topologies than torus ones. We conclude by discussing the feasibility of this approach to control polymer motion in biotechnology applications such as sequencing.

1 Introduction

Knots are found everywhere in our daily lives, whether they be fashion accessories or items to fasten two objects together. However, unknown to many people, knots also play an important role in biology. For example, knots in the umbilical cord create complications during child birth,[1] and knots in DNA alter the kinetics of transcription,[2] so much so that nature has evolved specific enzymes to control the topology of these chains.[3–5] Driven by these observations, there has been considerable interest in recent years to understand how these self-entanglements alter the physical properties of polymers at the molecular scale.[6–8] By now, we know that knotting in long polymer strands is mathematically inevitable.[9,10] This phenomenon leads to drastic changes in the polymer's dynamics (relaxation,[11,12] coil-stretch[13,14]) and its mechanical properties (rupture strength[15]). We are now at the stage where researchers can test recent theories[16–18] *via* single-molecule experiments. For example, researchers can now tie knots into actin filaments[19] or DNA[20] *via* optical tweezers, and others are able to create knotted conformations *via* application of an electric field.[21,22]

In this paper, we discuss how knotting on an open, linear chain alters the chain's motion through small pores. This process, known as translocation, has wide ranging applications in biology and biotechnology. Viruses eject their DNA into hosts through small pores in the cell membrane.[23,24] Similarly, nanopore sequencing consists of passing DNA through a thin hole *via* an imposed electric field. If the resulting electric signal is sensitive to chemical detail, this event can be used to read the sequence along the chain's backbone.[25–27] This idea, proposed by Deamer and co-workers[28–30] and now implemented by Oxford Nanopore,[31,32] is a promising next-generation technology as it allows long DNA reads with little to no chemical modification. Its single-molecule nature allows one to sample genetic heterogeneity among cell populations, which is ideal for detecting rare events such as the onset of cancer.

Currently, one limitation facing nanopore sequencing is that DNA moves too quickly through the pore, rendering the electric signal to be noisy.[27,30,33] There are several proposals in the literature to address this issue,[34–36] most of which involve binding proteins onto DNA to ratchet it through the pore or using exonucleases to hydrolyze the end of the chain one nucleotide at a time.[37–39] The idea we present here uses entanglements such as knots to retard the motion of the polymer. The advantage of this technique is that little chemical modification is required and it could be generalized to other polymer systems. As little has been examined on this front, we would like to

[a] *Department of Chemical Engineering, Massachusetts Institute of Technology, Cambridge, MA, 02139, USA. E-mail: pdoyle@mit.edu*
[b] *Liquiglide, 75 Sidney Street, Cambridge, MA, 02139, USA*

† Electronic supplementary information (ESI) available. See DOI: 10.1039/c6sm00545d

perform simulations to provide physical insight into this process.

Our paper is divided into two parts. First, we will discuss the translocation dynamics of a knotted polymer under constant field. Previous authors have simulated this process,[40,41] finding that knots completely halt translocation above a critical force. Suma *et al.*[41] also examined the effect that topology plays in this process, finding that twist knots jam more easily than torus knots. We verify these effects in our simulation, and we examine another phenomenon that has been unreported thus far. Close to the jamming transition, we find that the translocation speed exhibits large fluctuations because the knot's dynamics are extremely sensitive to its conformation as it enters the pore. These observations are evidence of caging, stick-slip motion, and molecular individualism[42–44] of a polymer knot. From a practical standpoint, these results state that there are force regimes where translocation will be difficult to control and thus should be avoided.

The primary contribution to this manuscript comes from the second part of the paper where we study the translocation dynamics of a knotted polymer when the applied field is periodic. We find that by cycling the field on and off at the relaxation time scale of the knot, we can control the swelling of the knot and hence ratchet the polymer through the pore. We examine how the translocation speed varies as a function of the cycle time. We also discuss limitations of this approach to control polymer motion. At large field amplitudes, we observe significant fluctuations in the translocation speed because the knot gets trapped in certain conformations during its relaxation. Remarkably, this effect appears most pronounced for particular chain topologies. We discuss the implication of these results in the conclusion.

We note that the glassy physics of locally-dense, single polymers have been receiving increasing attention in the scientific community. For example, recent experiments shown that collapsed DNA can jam at the pores of viral capsids.[45] It is of interest to manipulate these arrested states, and we hope to provide insight into tight, knotted systems here.

2 Methods

Fig. 1a shows the geometry of our Brownian dynamics simulations. We represent a polymer as a linear chain of N beads of diameter b connected by $N-1$ rods of length ℓ. The rod length ℓ is equal to the Kuhn length of a polymer, and we vary the bead diameter to alter the roughness along the polymer backbone, which gives rise to friction when segments slide over each other in an entanglement.[47] In the main manuscript, we will examine the situation when the bead diameter is equal to the rod length ($b = \ell$). In the ESI,† we will briefly discuss results when the beads are not touching ($b = 0.8\ell$, *i.e.*, more corrugated landscape) and slightly overlapping ($b = 1.5\ell$, *i.e.*, a smoother energy landscape). The model here is the simplest representation of a flexible polymer that captures the essential features of intra-chain friction.[48] It should yield order-of-magnitude estimates of jamming forces and time scales while summarizing the major

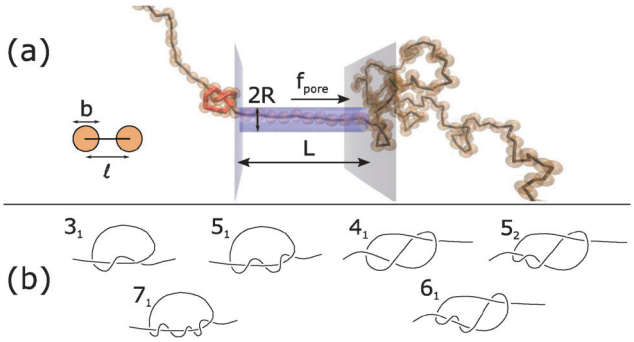

Fig. 1 (a) Schematic of Brownian dynamics simulation. A knotted polymer translocates through a pore with a force $f(t)$ per bead. (b) Types of knots simulated (Alexander–Briggs notation[46]).

trends in the translocation process. Note: if one were to more accurately determine the jamming behavior of a tightly knotted chain, one likely has to resort to all-atom, explicit solvent simulations to capture all the details of the short-range, intra-chain interactions. This task is computationally intensive and likely cannot be simulated for the time scales of interest here.

In our simulations, we tie a knot at the center of the chain and insert one end of the chain into a cylindrical pore of length L and radius R. Beads inside the pore are subject to a spatially-uniform but time-varying body force $f(t)$ along the pore's axis. This model, albeit simple, is a commonly-used, low-order representation of a polymer electrophoresing through a pore.[40,49–51] We simulate a chain of $N = 200$ beads and set the pore's radius and length to be $R = \ell$ and $L = 10\ell$. This way, a jammed knot of size 10–20 beads will be much smaller than the polymer chain but larger than pore's diameter, which will allow jamming to occur at sufficiently large forces. Like in previous studies,[40,49,52,53] we neglect hydrodynamic interactions between chain segments and set the drag coefficient of each bead to be ζ. Thus, the length and time scale of the problem are the rod size ℓ and its diffusion time $t_d = \ell^2\zeta/kT$, where kT is the thermal energy. Typical values for single-stranded DNA are $b = \ell = 1$ nm (its nominal width[40,41]) and $t_d = \ell^2\zeta/kT \approx 3\pi\eta\ell^3/kT \approx 2.3$ ns. To enforce the excluded volume interactions between chain segments, we apply a stiff harmonic potential between overlapping beads with spring constant $H = 5000\ kT/\ell^2$. Similarly, we localize the chain inside the pore by applying a repulsive harmonic potential on beads that overlap with the pore wall. More details can be found in the ESI,† including how we create the initial conditions.

In this paper, we vary the body force $f(t)$ in time and see how this parameter affects the velocity of the knotted polymer through the pore. The forces we apply are between $f = 1$–$20\ kT/\ell$. If we assume the effective, screened charge across 1 nm of single-stranded DNA is $q = -1.25e$, these forces correspond to a voltage drop of 0.20–4.1 V across the nanopore, values that have been achieved experimentally.[54] See ESI† for more details, which is inspired by the analysis of van Dorp *et al.*[55] The signals we pulse have a off times around $20t_d \approx 46$ ns, values that have been attained in electroporation studies.[56] We also examine what role the chain's topology plays in the translocation dynamics. The knot types we study are in Fig. 1b. The 3_1, 5_1, and 7_1 knots

are torus knots, which are knots whose contour can be mapped onto a surface of a torus. The 3_1, 4_1, 5_2, and 6_1 knots are twist knots, which are created by taking a linear chain, forming a loop with any number of half turns, and then passing one chain end through the loop. We note that the 3_1 knot is a member of both families.

To measure the boundaries of the knotted region in our simulations, we employ two techniques. The first technique involves projecting the knot onto a plane parallel to the pore axis and then determining the smallest subset of crossings that retains the chain topology *via* computation of the Alexander polynomial.[57,58] Since there are many planes that satisfy this condition, we choose the plane that gives rise to the smallest knot size. When the knot is jammed at the pore wall, we can also use a simpler technique to obtain the knotted boundary. We start one bead into the pore and calculate its number of nearest neighbors, defined as the number of beads within a cutoff radius $R_{\text{cutoff}} = 1.2b$. We march left until $N_{\text{neighbors}} = 2$, at which we assign this bead as the left knot boundary. We typically use the simpler technique to calculate the knot's radius of gyration when it is jammed at the pore, although it can only be used in the situation when the knot is relatively tight and its topology is not too complex (as is here).

3 Results – constant force

Fig. 2a shows trajectories of a knotted polymer moving through a pore when the body force f is constant in time and the bead diameter is the same as the rod length ($b = \ell$). The y-axis is the fraction of polymer translocated, defined as $\phi = (L_0 - s)/L_0$, where s is the contour of the polymer that has not entered the pore region and L_0 is the total length of the polymer. The results plotted here are for the 4_1 topology – one of the more common knot types observed in bulk and in channels.[59] When the knot contacts the pore – as indicated by the bend in the graphs – the polymer slows noticeably as the knot acts an additional source of chain friction. At low applied forces ($f = 3\ kT/\ell$), the polymer traverses the pore at a constant speed, albeit slower than the unknotted case. At high forces ($f = 7\ kT/\ell$), translocation completely halts since the knot jams at the pore entrance. This qualitative behavior has been observed in simulations by Huang *et al.*,[60] Rosa *et al.*,[40] and Suma *et al.*[41] At very high forces, the knot becomes tight and the probability of polymer reptating through its core becomes exponentially small.[47]

At intermediate forces ($f = 5\ kT/\ell$), we observe qualitatively different behavior. Some trajectories are completely jammed, others move through the pore at uniform speed, while others exhibit stick-slip motion. In this situation, the configuration of the knot at the pore wall plays a large role in the chain's dynamics. Fig. 3a demonstrates an example of this effect. In this graph, we see a trace of one polymer with a 4_1 knot moving through a pore. The polymer switches between jammed and unjammed states, and during the transition, the radius of gyration of the knotted region makes distinct hops. The number of monomers in the knotted core changes as well. Results for the other knot topologies (3_1, 5_1, 5_2, 6_1) are shown in the ESI.† For the most part, we observe a broad distribution in the polymer's transit times when the knot is close to the jamming transition, although for other knot topologies, we see large fluctuations at other force values as well.

Fig. 3b plots the forces at which we observe significant stick-slip behavior for the 4_1 knot. This figure shows the fraction of time the polymer is jammed over an ensemble of 20–50 runs. When this fraction is $O(0.5)$, stick-slip is significant and hence polymer motion is difficult to control. Although this regime should avoided from a practical standpoint, it is interesting from a physical perspective since it is an example of caging[47,61] and molecular individualism[42–44] of the knot.

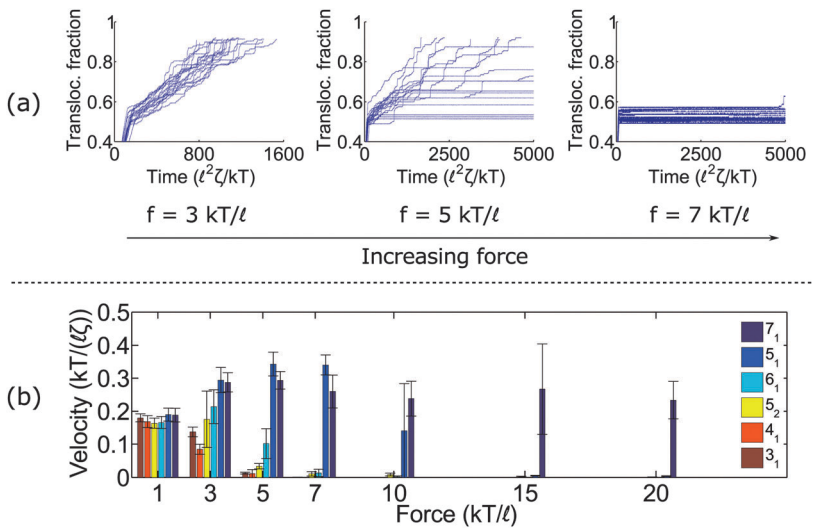

Fig. 2 Dynamics under constant force. (a) Traces of polymer translocation for a 4_1 knot. At low forces, the knots move through the pore at a nearly constant velocity. At high forces, the knot jams and halts the polymer's motion. At intermediate forces, large fluctuations are observed in the polymer translocation. For all plots, we show traces from 20 runs. (b) Average velocity as a function of force for different knot types. Non-twist knots (7_1 and 5_1) jam at much larger forces than twist knots (3_1, 4_1, 5_2, and 6_1). Error bars are standard deviations. The results here are for the case when the bead diameter is equal to the rod length ($b = \ell$).

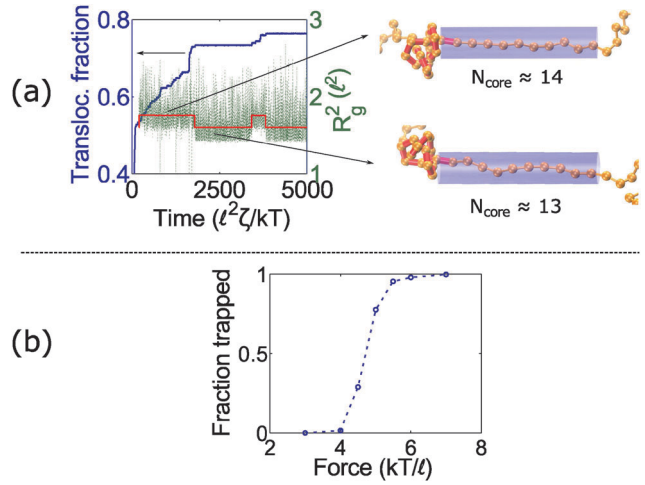

Fig. 3 Stick-slip motion of knotted polymers at intermediate forces. (a) Trajectory of a 4_1-knotted polymer under constant force ($f = 5\ kT/\ell$). When the motion stalls, the knot's radius of gyration makes a distinct hop. The red line is a piece-wise constant fit to the radius of gyration. Right: Snapshots of the knot show that the number of monomers in the knotted core changes during stick-slip motion. The bead size is equal to the rod length ($b = \ell$), but the beads are drawn small for illustrative purposes. (b) Fraction of time a knot is trapped as a function of force for the 4_1 topology. We consider a knot trapped if it moves less than 0.4ℓ for times greater than $250\ \ell^2\zeta/kT$. The data points are averages over 20–50 runs.

We close this section by graphing the mean translocation speed $\langle v \rangle$ as a function of applied force f for several different knot topologies (Fig. 2b). We measure this quantity by fitting each polymer trajectory like in Fig. 2a to a straight line after the knot contacts the pore. We calculate the mean and standard deviation from 20 runs. One observation from these results is that the twist knots (3_1, 4_1, 5_2, and 6_1) jam much more easily than non-twist knots (5_1 and 7_1). This corroborates the observations by Suma *et al.*,[41] and that paper gives an elegant mechanistic explanation for why this discrepancy exists. In short, the twist knots dissipate tension much more easily than non-twist knots, which leads to less force being transmitted to the chain outside the pore. One difference in our graph is that we examine a larger dynamic force range (*e.g.*, we see that the 5_1 knot eventually jams). We also plot error bars, so one can see what forces lead to large fluctuations relative to the mean (see $f = 5\ kT/\ell$ for the 4_1 knot, $f = 7\ kT/\ell$ for the 5_2 knot, and $f = 10\ kT/\ell$ for the 5_1 knot). We note that the values of jamming we obtain in this study are larger than the ones reported by Suma *et al.*[41] This result can be expected as we use nearly hard-sphere repulsions to enforce excluded volume interactions while the other authors use softer intra-chain interactions that allow knots to tighten more easily. We also use a larger pore diameter ($R = \ell$ as opposed to $R = 0.775\ell$).

In the ESI,† we examine how the roughness of the polymer backbone alters the jamming physics. As expected, knots with a more corrugated backbone ($b = 0.8\ell$, *i.e.*, non-touching beads) jam at lower forces than ones with a less corrugated backbone ($b = \ell$, *i.e.*, touching beads). If the backbone is fairly smooth ($b = 1.5\ell$, *i.e.*, overlapping beads), the knots jam at very large forces for certain topologies but fail to jam for other topologies. In the next section, we will see that the corrugation plays a large role in relaxation behavior of the knot – *i.e.*, how the knot swells from its tightened state.

4 Results – pulsed force field

In the previous section, we found that knotted polymers jam at the pore's entrance above a critical force. This observation presents a method to control the motion of the polymer by cycling the applied force. Fig. 4a and b shows the schematic of this idea. We apply force f_1 above the jamming transition for time τ_1, followed by zero force for time τ_2, and then repeat this process *ad-infinitum*. During the first part of the cycle, the knot jams at the pore entrance and halts the polymer's motion. During the relaxation cycle τ_2, the knot swells and diffuses away from the pore. This process introduces slack into the chain, which allows it to ratchet through the pore when the force is turned back on. Thus, by controlling the relaxation dynamics of the chain, one can manipulate the polymer's speed.

We demonstrate this claim in Fig. 4c and d. In Fig. 4c, we plot the trajectories of a polymer with a 3_1 knot under a pulsed field with parameters $f_1 = 7\ kT/\ell$ and $f_2 = 0\ kT/\ell$. We vary the time τ_2 spent in the off-cycle but keep the total cycle time $\tau_1 + \tau_2$ to be constant ($\tau_1 + \tau_2 = 100\ \ell^2\zeta/kT$). The bead size is equal to the rod length ($b = \ell$). In the figure, we see that the polymers traverse through the pore in a step-wise fashion with the mean velocity increasing with increasing time spent in the off-cycle. We plot the average translocation speeds of 3_1 and 4_1 knots in Fig. 4d, the knots most commonly found *in vitro*.[62] Again, we can tailor the average speed at which polymers move through the pore, and furthermore, these speeds are demonstrably slower than the free chain case (Fig. 4d inset). Translocation speeds for other knot topologies are shown in the ESI.†

How does cycling the force field affect the fluctuations in the polymer's speed? In some situations, the cycling will reduce the relative fluctuations, while in other situations it will enhance them. We demonstrate the former in Fig. 5. In part (a), we plot trajectories of a polymer with a 6_1 twist knot when we cycle the force field between $f_1 = 7\ kT/\ell$ and $f_2 = 0\ kT/\ell$. We keep the total cycle time constant at $\tau_1 + \tau_2 = 100\ \ell^2\zeta/kT$ and vary the time τ_2 spent in the off cycle. We note that force f_1 for this topology is slightly below the jamming transition and hence leads to large fluctuations when the cycle time τ_2 is zero or nearly zero. However, when the off cycle is $\tau_2 = 20\ \ell^2\zeta/kT$, the fluctuations are suppressed and the translocation speed becomes fairly constant. The reason why this phenomenon occurs is that during the off part of the cycle, the knot swells considerably – more than the contour that reptates through the pore during the on cycle (Fig. 5b). Thus, the relaxation dynamics in this case swamp out any fluctuations that rise due to the knot contacting the pore.

In Fig. 6, we show a situation where the cycling gives rise to the opposite effect – *i.e.*, enhanced fluctuations. In this graph, we show the 3_1 and 4_1 knot moving through the pore when we cycle the force field between two values: $f = f_1$ and $f_2 = 0$. We vary the force f_1 during the on cycle but keep the cycle times the

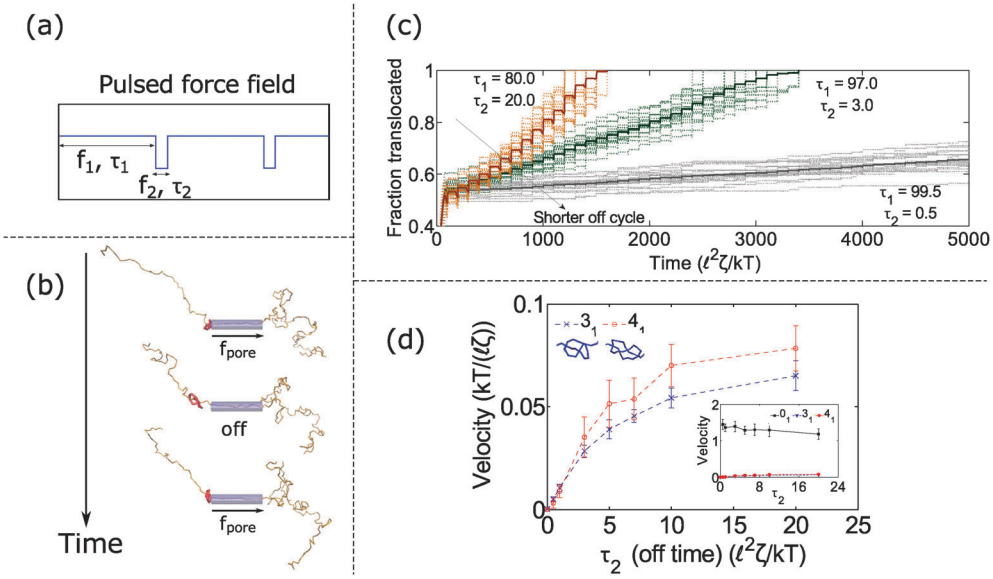

Fig. 4 Dynamics with oscillating force. (a) Periodic force profile applied to polymer inside pore. (b) Snapshots of polymer movement when we cycle the field on and off. The polymer jams during the on cycle and relaxes during the off cycle, which allows us to ratchet the polymer through the pore. (c) Trajectories of polymer translocation with a 3_1 knot. We alternate between a constant field ($f_1 = 7\ kT/\ell$) and no field ($f_2 = 0\ kT/\ell$). The total cycle time is fixed: $\tau_1 + \tau_2 = 100\ \ell^2\zeta/kT$. By adjusting the off time τ_2, we control the speed at which the polymer moves through the pore. Faint lines are trajectories from 20 runs, and dark lines are averages from these runs. (d) Average translocation speed *vs.* off time for the 3_1 and 4_1 knot. The inset shows the speed of the unknot (0_1). The parameters are $f_1 = 7\ kT/\ell$, $f_2 = 0\ kT/\ell$, $\tau_1 + \tau_2 = 100\ \ell^2\zeta/kT$. Error bars are standard deviations from 20 runs. All results are for the case when the bead diameter is equal to the rod length ($b = \ell$).

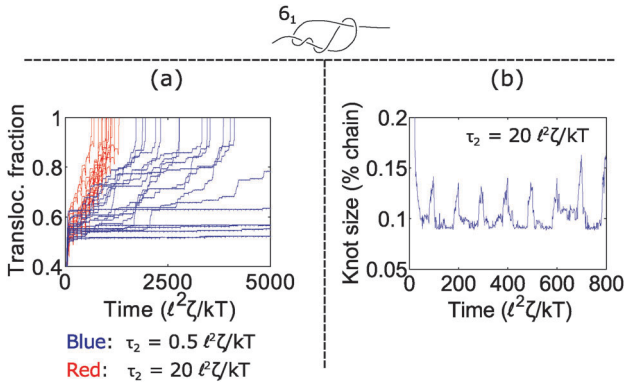

Fig. 5 Reduction of fluctuations near jamming transition. (a) Trajectories of a 6_1 knot when we cycle the force field on and off between $f_1 = 7\ kT/\ell$ and $f_2 = 0$. f_1 is close to the jamming transition for this knot topology. The total cycle time is $\tau_1 + \tau_2 = 100\ \ell^2\zeta/kT$ and we vary the off time τ_2. Increasing the off time reduces fluctuations in the polymer's transit time. (b) Knot size *vs.* time for one trajectory when the off time is $\tau_2 = 20\ \ell^2\zeta/kT$. The knot swells by 4% of the chain during relaxation, which is larger than the maximum amount of contour reptating through the knot in the constant force case (maximum 2% of chain). In all simulations, the bead size is equal to the rod length ($b = \ell$).

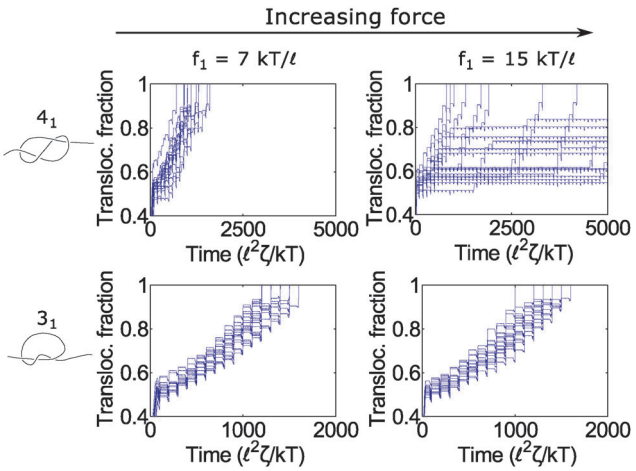

Fig. 6 Enhanced fluctuations due to cycling at large forces. Top row: Trajectories of a 4_1-knotted polymer moving through a pore *via* a force field cycling on and off. The on time is $\tau_1 = 80\ \ell^2\zeta/kT$, and the off time is $\tau_2 = 20\ \ell^2\zeta/kT$. At moderate forces ($f_1 = 7\ kT/\ell$), the polymer ratchets through the pore with a fairly constant velocity. If the force becomes too large ($f_1 = 15\ kT/\ell$), the polymer's speed exhibits large fluctuations. This phenomenon appears primarily for the non-torus knots (4_1, 5_2, 6_1) but not for the torus knots (3_1, 5_1, 7_1) (see ESI† for details). Bottom row: Trajectories of a 3_1 knot at the same forces. Here we do not observe large fluctuations. In these simulations, the bead size is equal to the rod length ($b = \ell$).

same at $\tau_1 = 80\ \ell^2\zeta/kT$ and $\tau_2 = 20\ \ell^2\zeta/kT$. The forces we examine are well above the jamming transition for the two knot topologies. When $f_1 = 7\ kT/\ell$, the polymers ratchet through the pore in a stepwise fashion with a fairly uniform velocity. When the applied force is very large ($f_1 = 15\ kT/\ell$), the 4_1 knot exhibits large fluctuations in its speed while the dynamics of the 3_1 knot stays the same. We observe such enhanced fluctuations for the non-torus knot topologies (4_1, 5_2, and 6_1) but have yet to observe these effects for the torus topologies (3_1, 5_1, 7_1) – see ESI† for more details. We offer an explanation for this phenomenon below.

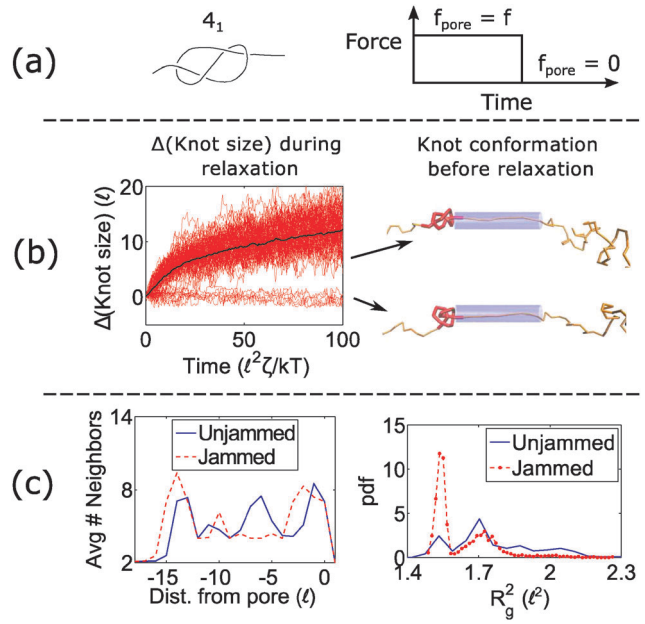

Fig. 7 Failure to unjam during relaxation. (a) We run a simulation of a 4_1 knot with the force profile on the right. f_{pore} = 15 kT/ℓ. The bead size is equal to the rod length ($b = \ell$). (b) During the relaxation process, the knot size swells for certain configurations but remains arrested for others (100 runs total). Representative snapshots of the knot before relaxation is shown on the right. Beads are removed for illustration purposes. (c) Average number of near-neighbors ($R < 1.2b$) and radius of gyration for the two populations (jammed *vs.* unjammed) before relaxation occurs.

When a knot jams at very large forces, it may become trapped in a metastable state with an escape potential of several kT. To verify this statement, we ran a simulation of a knotted polymer at the pore wall undergoing a step relaxation (Fig. 7a). The initial topology is a 4_1 knot, and the initial force is $f = 15\ kT/\ell$, *i.e.*, the force at which we observe large fluctuations when we cycle the field as in Fig. 6. When we turn off the field, we see that some trajectories of the 4_1 knot remain jammed while others swell easily (Fig. 7b). The knot's caging appears to be dependent on how it contacts the pore wall before the field is turned off. In Fig. 7c, we divide all knot trajectories into two populations – one that remains jammed during relaxation and one that remains unjammed. If we plot the average density profile of these two populations before relaxation begins, we see that the two profiles are distinct. We observe a similar distinction for the knot's radius of gyration (Fig. 7c) as well as a simple visual check of the knot's conformation (Fig. 7b). Videos of the step relaxation simulation are in the ESI.†

This caging phenomenon is highly dependent on knot topology and the friction along the polymer backbone. For the case when the bead size is equivalent to the rod length ($b = \ell$), we observe that torus topologies (3_1, 5_1, 7_1) relax normally while non-torus ones (4_1, 5_2, and 6_1) fail to unjam at large initial forces ($f \geq 15\ kT/\ell$). If the polymer backbone is more corrugated ($b = 0.8\ell$, *i.e.*, non-touching beads), this effect is more pronounced. However, if the polymer's backbone is fairly smooth ($b = 1.5\ell$, *i.e.*, overlapping beads), we find that the knots relax normally even at very large initial forces ($f = 40\ kT/\ell$). See ESI† for more details.

5 Discussion

In this study, we investigate the feasibility of using knots to slow down and control the translocation of polymers through nanopores. Under a constant, external field, we find that:

- Knots halt translocation above a critical force
- Twist knots (3_1, 4_1, 5_2, 6_1) jam more easily than non-twist knots
- For many topologies, polymers experience large fluctuations in their transit times when the knot is slightly below its jamming transition.

These observations show that polymer motion can be drastically altered by the friction created from self-entanglements. This friction is generated by chain segments sliding past each other in the knotted core, and the resistance to this motion depends on the short-range interactions in the knotted region as well as the tension at the pore entrance. The model we employ here is the simplest representation of a flexible chain that captures the essential features of this friction.[47] It treats the polymer backbone as an energy landscape corrugated at a monomer length scale, a result borne from recent optical tweezer experiments as the origin of solid friction between polymer filaments.[63] Thus, although we do not take into account all the short-range interactions in a polymer like single stranded DNA, we expect our model to capture the generic features of a translocation experiment and give order-of-magnitude estimates for the critical voltages required for jamming.

For the model we choose (the nominal chain width b is approximately equal to the Kuhn step ℓ), a voltage drop of roughly 1.4 V is needed to jam a 3_1 or 4_1 knot of ssDNA along a pore of 2 nm diameter and 10 nm depth. For more complex topologies (5_1, 6_1), double the voltage is needed. If experiments show that the transition occurs at a smaller voltage than expected, the energy landscape along the polymer backbone is more corrugated than the model suggests – *i.e.*, there is greater friction due to chains sliding past each other. In general, these experiments can provide insight into how friction arises between chain entanglements, an area that is receiving increasing interest in the polymer physics community as well as in studies with granular, macroscopic chains.[64,65] Furthermore, the stick-slip phenomenon observed in this manuscript is fascinating from a physics standpoint as it demonstrates how polymers under the same operating conditions exhibit vastly different dynamics depending on the knot's configuration. It is one of many examples of molecular individualism of a polymer strand[42–44] and it shows how topology plays a large role in the polymer's dynamical fluctuations.

In the second part of the manuscript, we examine the dynamics of a knotted chain when the external field is cycled on and off. If the off time is comparable to the relaxation time of the knot, we can adjust the swelling of the knot and hence ratchet the polymer through the pore. If we perform step relaxation simulations of knots (Fig. 8) and fit the knot size during relaxation to an exponential function $y = a[1 - \exp(-t/\tau_{knot})]$, we obtain a relaxation time of $t_{knot} \approx 20$–$35\ \ell^2\zeta/kT$ and a change in knot size of $a \approx 8 - 18\ell$ for the topologies studied so far (provided that the knots do not arrest during relaxation). This corresponds to

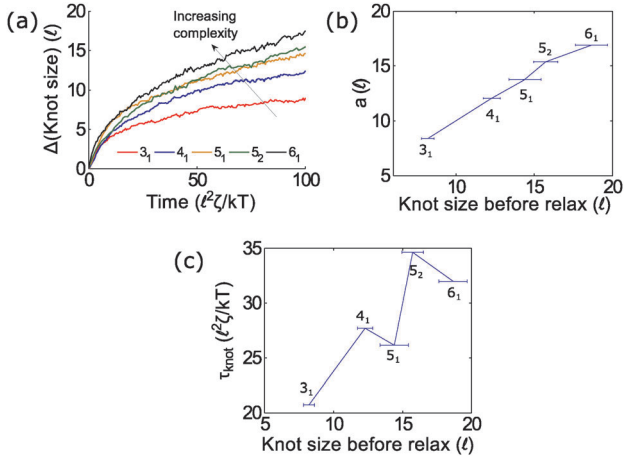

Fig. 8 Knot swelling during relaxation. (a) We perform simulations of knots undergoing a step relaxation and plot the knot size *vs.* time during the relaxation process. The initial force is above the jamming transition but small enough that the knots do not arrest during relaxation ($f = 7\ kT/\ell$ for the 3_1 and 4_1 knots, $f = 10\ kT/\ell$ for the 5_2 and 6_1 knots, and $f = 15\ kT/\ell$ for the 5_1 knot). Curves are ensemble averages for 50–100 runs. If we fit each curve to an exponential $y = a[1 - \exp(-t/\tau_{knot})]$, the best-fit coefficients for the change in knot size a and the knot-relaxation time τ_{knot} are in (b) and (c). In all simulations, the bead size is equal to the rod length ($b = \ell$).

a time scale of $t_{knot} \approx$ 40–70 ns and a change in knot size of 8–18 nm for single stranded DNA over the time scale studied (200 ns). We expect both of these quantities to increase for more complex topologies. We also expect the knot to swell further at much longer times to a metastable size of $\approx$140 monomers.[17]

When the initial tension on the chain is sufficiently large, the knot can arrest during relaxation. This effect is more pronounced for non-torus topologies than torus ones, and this effect can ultimately lead to large fluctuations in the polymer's transit times through the nanopore (Fig. 6). Again, we note that the forces at which we observe this phenomenon are dependent on the knot's internal friction, which in turn is dependent on the corrugated energy landscape along the polymer backbone. Our model predicts a voltage drop of approximately 3 V is needed across a pore of 2 nm diameter and 10 nm depth to observe the caging of the 4_1 and 5_2 knots during relaxation. If the polymer backbone is more corrugated than our model suggests, then this phenomenon will be more prominent. We also note that in some instances, the caging of the knot depends on the geometry of the knot just before it relaxes (Fig. 7c). This observation indicates that the knot's dynamics exhibit memory, which is an interesting topic to examine in the future.

In this work, we do not study how the pore size and the overall chain length alter the dynamics of the knotted polymer. The former is likely to modify the critical force for jamming, while the latter is likely to modify the polymer's speed, especially if the chain is large and long-range hydrodynamic interactions are included. These effects are ripe for future investigation. Additionally, it would be interesting to inspect how the charge relaxation inside the pore alters the knot's dynamics. In most solid state pores, the time scale of charge relaxation is $t_{cap} = R_s C_p$ = 75 ps to 1 μs,[66–68] where R_s is the resistance of the ionic solution and C_p is the pore's capacitance. If $t_{cap} > t_{knot}$, the knot will remain under tension during charge rearrangement and hence one will have to cycle at a time scale comparable to t_{cap}. Lastly, it is important to extend this study to semi-flexible chains such as double stranded DNA, since many sequencing applications utilize this polymer.

6 Conclusion

In this paper, we study the dynamics of a knotted polymer moving through a pore under an external field. We examine the dynamics when the field is constant in time and when the field periodically switches on and off. We find the latter case can be used to control the knot's swelling at the pore entrance and hence control the polymer's motion through the pore. We discuss how this strategy alters the fluctuations in the polymer's transit times. Cycling the field can reduce fluctuations near the knot's jamming transition, but can increase fluctuations at very large forces as the knot gets trapped in metastable states during relaxation. Although the predictions here have yet to be experimentally tested, we provide some order-of-magnitude estimates of voltages and cycle times where we expect knot jamming and ratcheting dynamics to occur. We also briefly address how the roughness along the polymer backbone alters the frictional dynamics of this system.

This study is interesting not only for applications such as nanopore sequencing, but it also provides insight into how self-entanglements give rise to friction in chains, an area of active research in the polymer physics community. This study also describes the relaxation behavior of a tight knot, which to this date has been unreported. This phenomenon may be important in direct optical mapping[69] where tight knots in genomic-length DNA appear as false deletions that obscure data analysis.[70] Other applications where entangled polymers move through pores include tertiary oil recovery,[71] chromatography, and virus-to-cell transmission.[72] Lastly, after initial submission of this work, Szymczak performed simulations of knotted proteins moving through pores.[73] Molecular motors apply forces in an on–off fashion, which allow these proteins to ratchet through pores in a manner similar to what we observe here.

Acknowledgements

This work is supported by the Singapore-MIT Alliance for Research and Technology (SMART) and National Science Foundation (NSF) grant CBET-1335938. We also thank Prof. Alfredo Alexander-Katz for fruitful discussions regarding this work.

References

1 W. Camann and J. Marquardt, *N. Engl. J. Med.*, 2003, **349**, 159.
2 J. Portugal and A. Rodriguez-Campos, *Nucleic Acids Res.*, 1996, **24**, 4890–4894.
3 A. J. Schoeffler and J. M. Berger, *Q. Rev. Biophys.*, 2008, **41**, 41–101.

4 J. C. Wang, *Annu. Rev. Biochem.*, 1996, **65**, 635–692.
5 J. J. Champoux, *Annu. Rev. Biochem.*, 2001, **70**, 369–413.
6 D. Meluzzi, D. E. Smith and G. Arya, *Annu. Rev. Biophys.*, 2010, **39**, 349–366.
7 C. Micheletti, D. Marenduzzo and E. Orlandini, *Phys. Rep.*, 2011, **504**, 1–73.
8 E. Orlandini and S. G. Whittington, *Rev. Mod. Phys.*, 2007, **79**, 611.
9 D. Sumners and S. Whittington, *J. Phys. A: Math. Gen.*, 1988, **21**, 1689.
10 E. J. Van Rensburg, D. Sumners, E. Wasserman and S. Whittington, *J. Phys. A: Math. Gen.*, 1992, **25**, 6557.
11 S. R. Quake, *Phys. Rev. Lett.*, 1994, **73**, 3317.
12 P. Y. Lai, Y. J. Sheng and H. K. Tsao, *Physica A*, 2000, **281**, 381–392.
13 C. B. Renner and P. S. Doyle, *Soft Matter*, 2015, **11**, 3105–3114.
14 D. Kivotides, S. Wilkin and T. Theofanous, *Phys. Rev. E: Stat., Nonlinear, Soft Matter Phys.*, 2009, **80**, 041808.
15 A. M. Saitta, P. D. Soper, E. Wasserman and M. L. Klein, *Nature*, 1999, **399**, 46–48.
16 A. Y. Grosberg and Y. Rabin, *Phys. Rev. Lett.*, 2007, **99**, 217801.
17 L. Dai, C. B. Renner and P. S. Doyle, *Phys. Rev. Lett.*, 2015, **114**, 037801.
18 L. Dai, C. B. Renner and P. S. Doyle, *Macromolecules*, 2015, **48**, 2812–2818.
19 Y. Arai, R. Yasuda, K. Akashi, Y. Harada, H. Miyata, K. Kinosita and H. Itoh, *Nature*, 1999, **399**, 446–448.
20 X. R. Bao, H. J. Lee and S. R. Quake, *Phys. Rev. Lett.*, 2003, **91**, 265506.
21 J. Tang, N. Du and P. S. Doyle, *Proc. Natl. Acad. Sci. U. S. A.*, 2011, **108**, 16153–16158.
22 C. B. Renner, N. Du and P. S. Doyle, *Biomicrofluidics*, 2014, **8**, 034103.
23 L. F. Liu, L. Perkocha, R. Calendar and J. C. Wang, *Proc. Natl. Acad. Sci. U. S. A.*, 1981, **78**, 5498–5502.
24 R. Matthews, A. A. Louis and J. M. Yeomans, *Phys. Rev. Lett.*, 2009, **102**, 088101.
25 S. Chang, S. Huang, J. He, F. Liang, P. Zhang, S. Li, X. Chen, O. Sankey and S. Lindsay, *Nano Lett.*, 2010, **10**, 1070–1075.
26 J. Clarke, H. C. Wu, L. Jayasinghe, A. Patel, S. Reid and H. Bayley, *Nat. Nanotechnol.*, 2009, **4**, 265–270.
27 C. Dekker, *Nat. Nanotechnol.*, 2007, **2**, 209–215.
28 J. J. Kasianowicz, E. Brandin, D. Branton and D. W. Deamer, *Proc. Natl. Acad. Sci. U. S. A.*, 1996, **93**, 13770–13773.
29 J. J. Kasianowicz, J. W. F. Robertson, E. R. Chan, J. E. Reiner and V. M. Stanford, *Annu. Rev. Anal. Chem.*, 2008, **1**, 737–766.
30 D. Branton, D. W. Deamer, A. Marziali, H. Bayley, S. A. Benner, T. Butler, M. Di Ventra, S. Garaj, A. Hibbs, X. Huang, S. B. Jovanovich, P. S. Krstic, S. Lindsay, X. S. Ling, C. H. Mastrangelo, A. Meller, J. S. Oliver, Y. V. Pershin, J. M. Ramsey, R. Riehn, G. V. Soni, V. Tabard-Cossa, M. Wanunu, M. Wiggin and J. A. Schloss, *Nat. Biotechnol.*, 2008, **10**, 1146.
31 E. C. Hayden, *Nature*, 2015, **521**, 7550.
32 A. Mikheyev and M. M. Y. Tin, *Mol. Ecol. Resour.*, 2014, **14**, 1097–1102.
33 M. Muthukumar, C. Plesa and C. Dekker, *Phys. Today*, 2015, **68**, 40–46.
34 B. M. Venkatesan and R. Bahsir, *Nat. Nanotechnol.*, 2011, **6**, 615–624.
35 D. Fologea, J. Uplinger, B. Thomas, D. S. McNabb and J. Li, *Nano Lett.*, 2005, **5**, 1734–1737.
36 S. W. Kowalczyk, D. B. Wells, A. Aksimentiev and C. Dekker, *Nano Lett.*, 2012, **12**, 1038.
37 D. Deamer, *Annu. Rev. Biophys.*, 2010, **39**, 79–90.
38 G. M. Cherf, K. R. Lieberman, R. Rashid, C. E. Lam, K. Karplus and M. Akeson, *Nat. Biotechnol.*, 2012, **30**, 344.
39 E. A. Manrao, I. M. Derrington, A. H. Laszlo, K. W. Langford, M. K. Hopper, N. Gillgren, M. Pavlenok, M. Niederweis and J. H. Gundlach, *Nat. Biotechnol.*, 2012, **30**, 349.
40 A. Rosa, M. Di Ventra and C. Micheletti, *Phys. Rev. Lett.*, 2012, **109**, 118301.
41 A. Suma, A. Rosa and C. Micheletti, *ACS Macro Lett.*, 2015, **4**, 1420–1424.
42 P. G. de Gennes, *Science*, 1997, **276**, 1999–2000.
43 T. Perkins, D. Smith, R. Larson and S. Chu, *Science*, 1995, **268**, 83.
44 T. T. Perkins, D. E. Smith and S. Chu, *Science*, 1997, **276**, 2016–2021.
45 N. Keller, S. Grimes, P. J. Jardine and D. E. Smith, *Nat. Phys.*, 2016, DOI: 10.1038/nphys3740.
46 D. Rolfsen, *Table of knots and links, Appendix C*, Publish or Perish Press, 1976.
47 V. Narsimhan, C. B. Renner and P. S. Doyle, *ACS Macro Lett.*, 2016, **5**, 123–127.
48 A. Ward, F. Hilitski, W. Schwenger, D. Welch, A. W. C. Lau, V. Vitelli, L. Mahadevan and Z. Dogic, *Nat. Mater.*, 2015, **14**, 583–588.
49 V. V. Palyulin, T. Ala-Nissilab and R. Metzler, *Soft Matter*, 2014, **10**, 9016.
50 K. Luo, T. Ala-Nissila, S. C. Ying and A. Bhattacharya, *Phys. Rev. Lett.*, 2007, **99**, 148102.
51 H. H. Katkar and M. Muthukumar, *J. Chem. Phys.*, 2014, **140**, 135102.
52 K. Luo, T. Ala-Nissila, S. C. Ying and R. Metzler, *Europhys. Lett.*, 2009, **88**, 68006.
53 M. Fyta, S. Melchionna, S. Succi and E. Kaxiras, *Phys. Rev. E: Stat., Nonlinear, Soft Matter Phys.*, 2008, **78**, 036704.
54 J. B. Heng, A. Aksimentiev, C. Ho, P. Marks, P. V. Grinkova, S. Sligar, K. Schulten and G. Timp, *Nano Lett.*, 2005, **5**, 1883–1888.
55 S. van Dorp, U. F. Keyser, N. H. Dekker, C. Dekker and S. G. Lemay, *Nat. Phys.*, 2009, **5**, 347–351.
56 S. J. Beebe and K. H. Schoenbach, *J. Biomed. Biotechnol.*, 2005, **4**, 297–300.
57 A. V. Vologodskii, A. V. Lukashin, M. D. Frank-Kamenetskii and V. V. Anshelevich, *Zh. Eksp. Teor. Fiz.*, 1974, **66**, 2153–2163.
58 P. Virnau, *Phys. Procedia*, 2010, **6**, 117–125.
59 E. Orlandini and C. Micheletti, *J. Biol. Phys.*, 2013, **39**, 267–275.

60 L. Huang and D. E. Makarov, *J. Chem. Phys.*, 2008, **129**, 121107.
61 L. Huang and D. E. Makarov, *J. Phys. Chem. A*, 2007, **111**, 10338–10344.
62 V. V. Rybenkov, N. R. Cozzarelli and A. V. Vologodskii, *Proc. Natl. Acad. Sci. U. S. A.*, 1993, **90**, 5307–5311.
63 A. Ward, F. Hilitski, W. Schwenger, D. Welch, A. W. C. Lau, V. Vitelli, L. Mahadevan and Z. Dogic, *Nat. Mater.*, 2015, **14**, 583–588.
64 A. Belmonte, M. J. Shelley, S. T. Eldakar and C. H. Wiggins, *Phys. Rev. Lett.*, 2001, **87**, 114301.
65 E. Ben-Naim, Z. A. Daya, P. Vorobeiff and R. E. Ecke, *Phys. Rev. Lett.*, 2011, **86**, 1414.
66 G. Sigalov, J. Comer, G. Timp and A. Aksimentiev, *Nano Lett.*, 2008, **8**, 56–63.
67 M. Krems, Y. V. Pershin and M. Di Ventra, *Nano Lett.*, 2010, **10**, 2674–2678.
68 R. M. M. Smeets, U. F. Keyser, N. H. Dekker and C. Dekker, *Proc. Natl. Acad. Sci. U. S. A.*, 2008, **105**, 417–421.
69 E. T. Dimalanta, A. Lim, R. Runnheim, C. Lamers, C. Churas, D. K. Forrest, J. J. de Pablo, M. D. Graham, S. N. Coppersmith, S. Goldstein and D. C. Schwartz, *Anal. Chem.*, 2004, **76**, 5293–5301.
70 J. G. Reifenberger, K. D. Dorfman and H. Cao, *Analyst*, 2015, **140**, 4887–4894.
71 S. Rodriguez, C. Romero, M. L. Sargenti, A. J. Müller, A. E. Sáez and J. A. Odell, *J. Non-Newtonian Fluid Mech.*, 1993, **49**, 63–85.
72 W. Mothes, N. M. Sherer, J. Jin and P. Zhong, *J. Virol.*, 2010, **84**, 8360–8368.
73 P. Szymczak, *Sci. Rep.*, 2016, **6**, 21702.